Spatial and temporal stimulus variants for multifocal pupillography of the central visual field

Faran Sabeti *, Andrew C. James, Ted Maddess

ARC Centre of Excellence in Vision Science and Centre for Visual Sciences, Research School of Biology, The Australian National University, Canberra ACT 0200, Australia

ABSTRACT

Multifocal pupillographic objective perimetry (mfPOP) has the advantage of being a non-invasive, objective method for measuring up to 88 visual field responses from both eyes concurrently within 5 min. To date mfPOP has been used to assess the peripheral visual field. Here we examine the practicality of mfPOP for testing the macular region of the visual field. This study examines variations in temporal presentation rate, spatial stimulus layout and luminance intensity in a group of normal subjects to determine the optimal parameters for achieving high signal to noise ratios for a macular version of mfPOP. Responses to multifocal stimuli comprising 24 or 44 stimulus regions per eye were measured dichoptically achieving median signal to noise ratios of 2.47 z-score units. Long stimulus presentation intervals combined with 24 region non-overlapping layouts produced the largest contraction amplitudes and shortest response delays.

© 2010 Elsevier Ltd. All rights reserved.

1. Introduction

The current clinical standard for assessing function across the visual field is static automated perimetry (SAP), which is based on stimuli from the 1945 Goldmann perimeter (Wong & Sharpe, 2000). SAP relies heavily on subject attention; consequently, reliability and repeatability impose inherent limitations upon this method. Fatigue affects, fixation losses and unacceptable levels of false positives and negatives that lower sensitivity and specificity have been associated with SAP (Budenz et al., 2002; Henson, Evans, Chauhan, & Lane, 1996; Joson, Kamantigue, & Chen, 2002). High intra-test and test–retest variability is also present impairing the efficacy in using perimetry for monitoring progression of ocular disease (Artes, Iwase, Ohno, Kitazawa, & Chauhan, 2002; Chauhan & Johnson, 1999; Heijl, Lindgren, & Lindgren, 1989). Media opacities in the elderly also diminish the advantages gained from utilizing short-wavelength or high spatial frequency stimuli (Chen & Budenz, 1998; Kim, Kim, Shin, Kim, & Jung, 2001). The clinical application of objective perimetry has recently gained momentum in an effort to circumvent many of the sources of error found in SAP (Goldberg, Graham, & Klistorner, 2002; Hood & Zhang, 2000; Hood, Zhang et al., 2000; Lai et al., 2007). The challenges facing these methods have been low signal to noise ratios (SNRs), long setup times (Bjerre, Grigg, Parry, & Henson, 2004; Hood & Greenstein et al., 2000) and inter-subject variability (Klistorner & Graham, 2000).

Recently, perimetric techniques have been applied to pupil responses with varying results (Bergamin, Zimmerman, & Kardon, 2003; Hong, Narkiewicz, & Kardon, 2001). The advantages of this method of objective perimetry stem from its short setup and testing duration, and non-invasiveness. Investigations into the viability of pupil perimetry in mapping the visual field have shown promise (Hong et al., 2001; Kardon, Kirkali, & Thompson, 1991). Attempts have been made to use multifocal stimulation techniques to determine visual field sensitivity across a number of varying regions (Sutter & Tran, 1992). Field loss identified by multifocal pupillographic objective perimetry (mfPOP) has been shown to be highly correlated with visual field loss in patients with retinal diseases (Tan, Kondo, Sato, Kondo, & Miyake, 2001; Wilhelm et al., 2000). The authors found that slower presentation rates than are used in mfERG and mfVEPs produced larger pupillary responses. Recently, Maddess and co-workers (Bell, James, Kolic, Essex, & Maddess, 2010; Maddess, Bedford, Goh, & James, 2009a) reported high diagnostic accuracy of mfPOP in glaucoma and early stage diabetic retinopathy. Their novel technique utilized temporally and spatially sparse stimuli, meaning that any given stimuli tends not to have neighboring stimuli in space or time (James, Maddess, Goh, & Winkles, 2005a; James, Ruseckaite, & Maddess, 2005b; Maddess, James, & Bowman, 2005). While this technique is in its infancy, producing a technique that can reveal functional deficits from clinically invisible change remains paramount for improving diagnosticity and disease monitoring. A recent mfPOP study of Type II diabetics suggests this may be possible (Bell et al., 2010).

The purpose of this investigation is to determine the optimal stimulus conditions for achieving high SNRs for applications in a clinical setting. Earlier studies from this group used stimuli within the central 30° of fixation (Bell et al., 2010; Maddess et al., 2009a), here we were interested in whether mfPOP could be used for more

* Corresponding author. Fax: +61 02 6125 3808.
  E-mail address: faran.sabeti@anu.edu.au (F. Sabeti).

central defects. We also wanted to determine the effect of saturation on pupil response profiles in normal subjects from multifocal stimuli. Evidence of pupil response saturation to high stimulus contrasts have been demonstrated (Hong et al., 2001; Maddess et al., 2010; Young & Kennish, 1993). This information is important as saturation may limit measurement of milder changes in visual field sensitivity.

2. Methods

2.1. Subjects

Three experiments were undertaken each with eight normal volunteers (four males; four females), aged 21–45 years old (28 ± 7.4). Subjects were required to have no significant media opacity or other ocular disorders, have no systemic conditions to affect the eye or visual pathway and not receiving any medications known to affect the pupil responses. Best corrected visual acuities were required to be at least 20/20 in each eye, normal fundus examination, and normal C-20 Frequency Doubling Perimetry. The study adhered to the requirements of the Australian National University's Human Experimentation Ethics Committee (protocol 04/238) and written informed consent was obtained from each subject prior to testing.

2.2. Stimuli

Dichoptic multifocal stimuli presented on two LCD displays at optical infinity were arranged in a dartboard layout (Fig. 1) with blurred margins to reduce the affects of refractive error on responses. This technique allowed each eye to receive independent stimulus presentations (dichoptic stimulation) generating direct and consensual pupil responses concurrently from every retinal region. In addition, this allowed for afferent and efferent defects to be discriminated at all visual field locations (Bell et al., 2010). The background was 10 cd/m^2 had a small central fixation cross. Steps were taken to maintain fusion that included an initial adjustment of ocular vergence to suit the subjects distance phoria and a long thin vertical white line bisecting the fixation point. The backgrounds for both eyes contained a dim starburst, radial grating pattern, which also helped maintain fusion. Stimuli were presented on a pair of LCD displays with a 60 frame/s refresh rate. Stimulus size was scaled with eccentricity in an attempt to balance the regional response sizes. Experiment 1 (Table 1) consisted of six stimulus protocols with yellow stimuli transiently (33 ms) presented at a luminance of 210 cd/m^2 extending to 10° eccentricity from fixation.

The mean interval of stimulus presentation at each region was either 1, 2 or 4 s between presentations (LS, S, MS respectively); with each interval being presented in both a 44 and 24 test region ensemble format (Fig. 1A and B). The combination of dichoptic stimuli (i.e. no binocular stimuli presented on any frame), and the low mean rate of presentations at each visual field region, mean that binocular rivalry was unlikely to have had a significant effect (James et al., 2005b; Maddess et al., 2005). The 44 region array exhibited overlapping locations (Fig. 1A) but there was no overlap across the horizontal or vertical midlines, and no stimuli which overlapped were ever presented simultaneously. Experiment 2 (Table 1) followed identical protocol parameters with the exception that the stimulus array was scaled to extend to 15° eccentricity. Experiment 3 varied the stimulus luminances in the
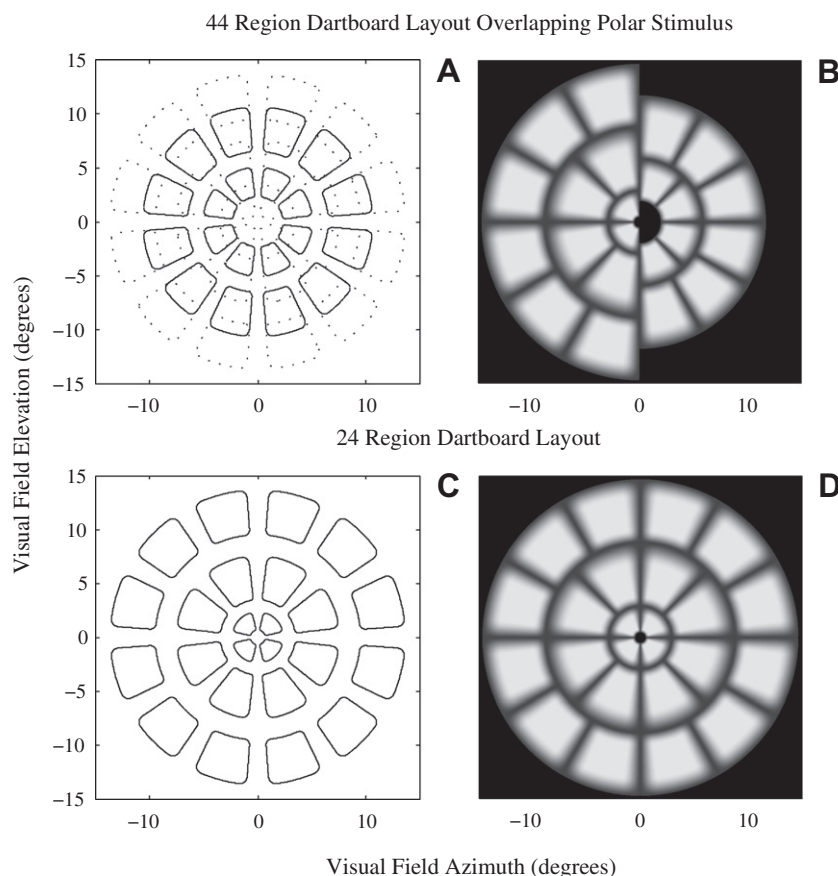

Fig. 1. Multifocal stimulus ensembles arranged in a dartboard layout shown as if all regions were on simultaneously which never happened in practice. (A and B) The 44 region layout had five rings of yellow overlapping polar stimuli shown as contour plots and as an image. The stimuli do not overlap across the horizontal and vertical midlines and stimuli which overlap in their skirts are never presented simultaneously. (C and D) The 24 region ensemble arranged in three non-overlapping rings. In both cases the stimuli were blurred (B and D) to reduce the effects of mis-refraction.

Table 1
Stimulus protocol characteristics.

Experiment 1: Subtending ± 10° of the visual field Experiment 2: Subtending ± 15° of the visual field				
Stimulus protocol	Stimulus (cd/m^2)	Background (cd/m^2)	Mean interval (s/region)	Regions/eye (Fig.1)
Least sparse 44 region pulse (LS44)	210	10	1	44
Sparse 44 region pulse (S44)	210	10	2	44
Most sparse 44 region pulse (MS44)	210	10	4	44
Least sparse 24 region pulse (LS24)	210	10	1	24
Sparse 24 region pulse (S24)	210	10	2	24
Most sparse 24 region pulse (MS24)	210	10	4	24

following manner: 48, 96,144, 192, 240, 288 cd/m^2. Otherwise all stimulus parameters were fixed to yellow elements presented at a mean interval of four presentations/s/region with 44 test regions, subtending the central 15° of the visual field.

2.3. Procedure

The mfPOP technique has been described in detail elsewhere (Bell et al., 2010; Maddess et al., 2009a); the following is a brief summary of the methods employed in this study. All subjects were tested with a prototype of the FDA cleared Truefield Analyzer (Seeing Machines Ltd., Acton, ACT Australia). Each experiment was divided into two testing sessions. The order of protocols were randomized and three protocols were tested at each subject visit. Each protocol consisted of eight segments of 30 s test duration. Between each segment the subject was given a short rest break to blink, and recover from asthenopia, making the test duration approximately 5 min. Pupil responses were recorded with video cameras under infrared illumination and tracking of pupil diameter was achieved by fitting a circle to the lower 3/4 of the pupil margin. The analysis method meant that only segments with fixation losses or blinks in excess of 15% need to be repeated.

2.4. Analysis

The data was analyzed using Matlab (The Mathworks, Natick, MA). Mean pupil responses for each region were measured by a multiple regressive technique that provided standard errors for all contraction amplitudes and delays (Bell et al., 2010; Maddess et al., 2009a). Signal to noise ratios (SNRs) were determined by the ratio of the peak response on its standard error. Stimulus response curves from Experiment 3 were fitted to median contraction amplitudes over a range of luminance intensities using a Naka–Rushton equation:

$$r = \frac{r_{max}}{1 + \left(\frac{s}{s_h}\right)^{-z}} \tag{1}$$

where r is the response, r_{max}, the maximum possible response, s is the stimulus, s_h is the stimulus eliciting a half-maximal response, z is an exponent, and for $z > 1$ the response functions are sigmoidal.

3. Results

3.1. Effect of stimulus field size on multifocal pupillary responses

Each region of the ensemble was independently stimulated for each eye generating separate direct and consensual responses. Fig. 2 shows an example of multifocal pupillary responses recorded from both eyes of a normal subject to a 44 region stimulus (LS44) producing 176 responses per experimental protocol, including the direct and consensual responses. We found that the pattern of responses were similar for all protocols with larger responses measured in the temporal visual field than the nasal field, which is in
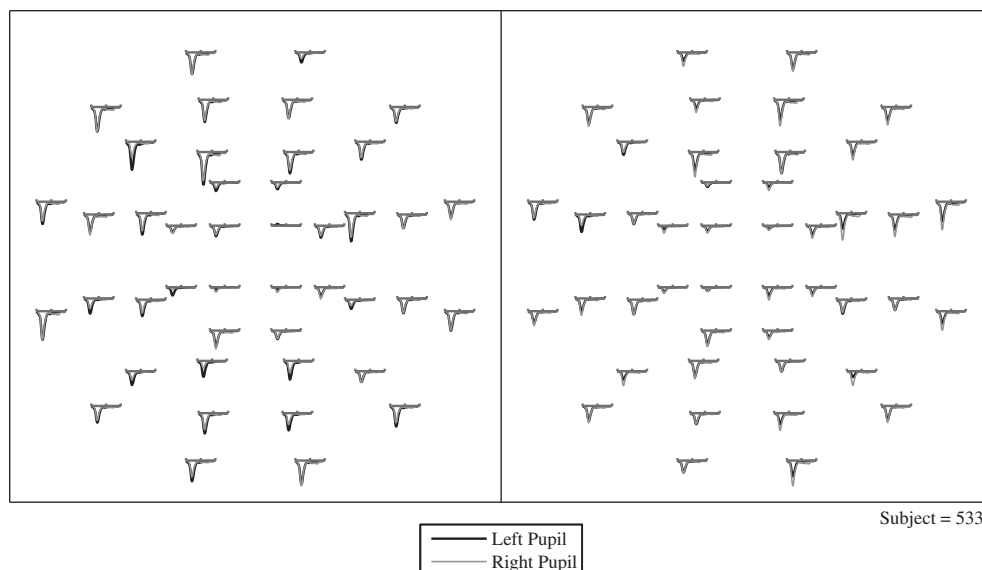

Subject = 533

— Left Pupil
— Right Pupil

Fig. 2. Example of direct and consensual pupillary recordings of a single test subject to yellow 210 cd/m^2 stimulus flashes (protocol ± 15°S44). Eighty-eight response waveforms were measured from each eye (OS at left) and their position corresponds approximately to the stimulus location in the visual field. Each waveform represents the mean response to the stimuli presented at that position. Direct and consensual responses were very similar and so mostly overlap. Waveforms were exclusively negative, representing pupillary contractions, with somewhat larger amplitudes observed in the temporal regions of the visual field.

agreement with past reports (Bell et al., 2010; Cox & Drewes, 1984; Maddess et al., 2009a; Smith & Smith, 1980). To confirm that visual field defects can be reproduced by mfPOP we examined the responses to a stimulus ensemble with one region unilaterally removed. The pupillary response waveform corresponding to the covered region was absent and the effect from a second repeat did not reach significance (-0.89 ± 0.66 μm, $P < 0.2$).

Given that the stimuli of Experiments 1 and 2 only differed in spatial scale the data are analyzed together in this section. The basic results are illustrated for the Experiment 2 data only in Fig. 3A and C showing the median peak constriction amplitude and median time to peak for those six stimulus protocols. In these figures it is apparent that temporally sparse non-overlapping 24 region stimuli yielded the largest peak contraction amplitudes at 10.31 ± 5.25 μm (median ± median absolute deviation). Median time to peak contraction (Fig. 3C) was also markedly shorter for stimulus protocol MS24 (460 ± 45 ms). The responses to the stimulus ensembles of Experiment 1 (all subtending ±10° of visual field) showed similar trends (6.36 ± 4.51 μm and 488 ± 54 ms, figure not shown). A more quantitative comparison of the independent effects that determined the responses will be given below.

Fig. 3 also shows SNRs that are expressed as *t*-statistics; due to the large number of responses these were essentially *z*-scores. The best *z*-score SNR for constriction amplitude computed across pupils, eyes, stimulus regions, and test subjects ($N = 1408$) was 2.47 ± 1.14 (mean ± SE) by protocol MS24 (Fig. 3B). Overall sparser stimuli with fewer regions tended to generate larger SNRs.

The independent effects of stimulus and subject parameters in Experiments 1 and 2 were quantified by the fitting of a multivariate linear model to decibel ($10\log_{10}$) transformed response amplitude data. The decibel transformation stabilized the variance and permitted multiplicative effects to be fitted. Strictly the response amplitudes were standardized as previously described (Bell et al., 2010; Maddess et al., 2009a). The regression model utilized a reference variable that represented the mean direct pupillary response (computed across eyes, pupils and visual field regions) of male subjects for stimulus protocol ± 10 °LS44. The significance of the difference of factors such as the mean amplitudes for each of the other protocols was determined by fitting it as a *contrast* to the reference value. Given the decibel transformation, each fitted factor represents the multiplicative increase or decrease in contraction amplitude for each protocol. This model matches the data given that a given stimulus condition provided responses that were some multiplicative factor, e.g. 10%, larger or smaller across all subjects. Table 2 summarizes the reference value, 3.68 ± 0.70 dB, and two parameters in the model but which do not relate to protocol, i.e. they are the average values across protocols: these are the effect of consensual responses (relative to direct), and the effect of being female. We did examine protocol-wise effects for gender and consensual but they were similar and so we simply show the mean effect here. On average consensual responses were smaller than direct by -0.41 ± 0.20 dB (0.91 times, $P < 0.05$). Females produced larger responses than males by 0.86 ± 0.20 dB (1.2 times, $P < 0.0001$). This is in agreement with a previous study, which also describes the linear model and other aspects of our analysis in more detail (Bell et al., 2010). The factors indicating the difference of the mean responses for the other 11 protocols compared to protocol ± 10 °LS44 are shown in Fig. 4. Protocols that have significantly larger mean responses are shown as black bars (Fig. 4A).

Experimental protocol ± 15° MS24 on average had the largest effect on pupillary contractions by 10.59 ± 0.33 dB ($P < 0.0001$). Fig. 4 shows that responses to ± 10° stimuli were smaller than
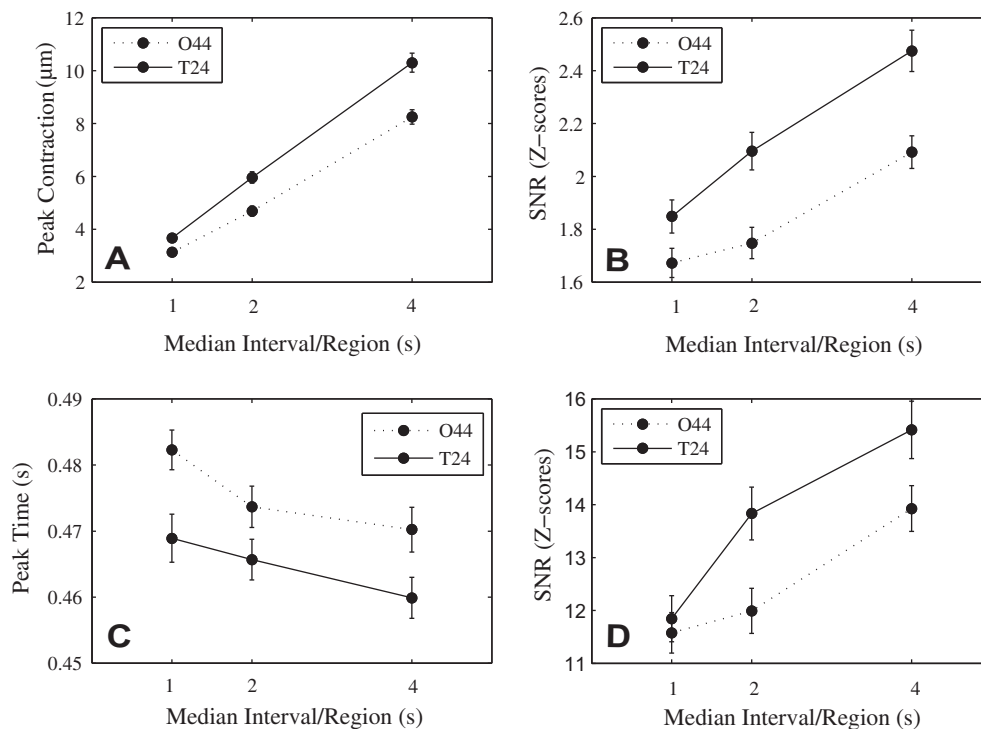

Fig. 3. (A) Median constriction amplitudes of the pupils were calculated across pupils, eyes, test regions, and subjects ($N = 1408$) for the overlapping 44 region (O44) and 24 region (T24) stimulus conditions subtending ± 15° radius visual field. (B) Median signal to noise ratios (SNRs) for the amplitudes expressed as *z*-scores of a normal distribution. Both amplitude and SNR indicate that the overlapping 24 region stimulus at a mean presentation interval of 4 s/region generate the largest responses. Error bars are SE. (C) Median time to peak response of the pupils were calculated for O44 and T24 stimulus conditions subtending a ±15° visual field. (D) Median SNRs expressed as *z*-scores calculated from peak time responses provides further evidence that 24 region stimulus out performs 44 region stimulus across multiple components of the pupillary waveforms.

Table 2
Pupil constriction amplitudes for Experiments 1 and 2 estimated by a multivariate linear model. The effect values represent deviations from the responses to the reference stimulus amplitude (dB) transformed (10log 10) to multiplicative gains.

Variable	dB	SE	t-stat	p
Reference (±10 °LS44)	3.68	0.70	5.23	1.92E − 07
Consensual	−0.41	0.20	−1.99	4.65E − 02
Female	0.86	0.20	4.21	2.67E − 05

those to ±15° stimulus arrays (Fig. 4A) and a separate analysis identified these two data sets to be significantly different ($P < 0.0001$).

Analyses of the effect of protocol variables on time to peak contraction were also undertaken. A similar model was fitted to the data but inspection of the results (Fig. 4B) did not show a difference in delay for larger versus smaller stimulus ensembles as found for contraction amplitudes (Fig. 4A). The mean (reference) delay was 550 ± 4.31 ms and the effect of the consensual response on latencies did not reach significance. Stimulus protocol ± 10° LS24 had the greatest effect on reducing time to peak on average by −40.87 ± −12.27 ms ($P < 0.0001$).

3.2. Effect of luminance level

Fig. 5A illustrates the median contraction amplitudes of the eight normal subjects over a range of stimulus intensities of yellow light. Saturation of pupil responses was determined from *stimulus response curves*. The Naka–Rushton equation (Eq (1)) was used to fit a sigmoid curve to the data and proved to be an excellent fit of the stimulus function for the pupil light reflex ($R^2 = 0.99$, $P < 0.0001$). On the assumption that the response should go to 0 when the stimulus strength was 0 we fitted the response versus stimulus luminance contrast (Fig. 5A), although fits to the stimulus luminance were not very different (e.g. Fig. 5B). The best fits, in terms of mean square errors, were obtained for exponents of $z = 1.4$, and a half-maximal stimulus, s_h, corresponding to a luminance of 210 cd/m². The R_{max} values were 11.7 μm for the left eyes and 12.0 μm for the right eyes. Similarly, it is apparent that the SNRs begin to plateau at higher stimulus luminances (Fig. 5B). These functions did not obviously have a sigmoidal shape so we characterized the saturation by fitting a power function of the form $R = kS^z$, where the exponent was 0.55, $z < 1$ indicating saturation. This result is in agreement with a much larger study that found
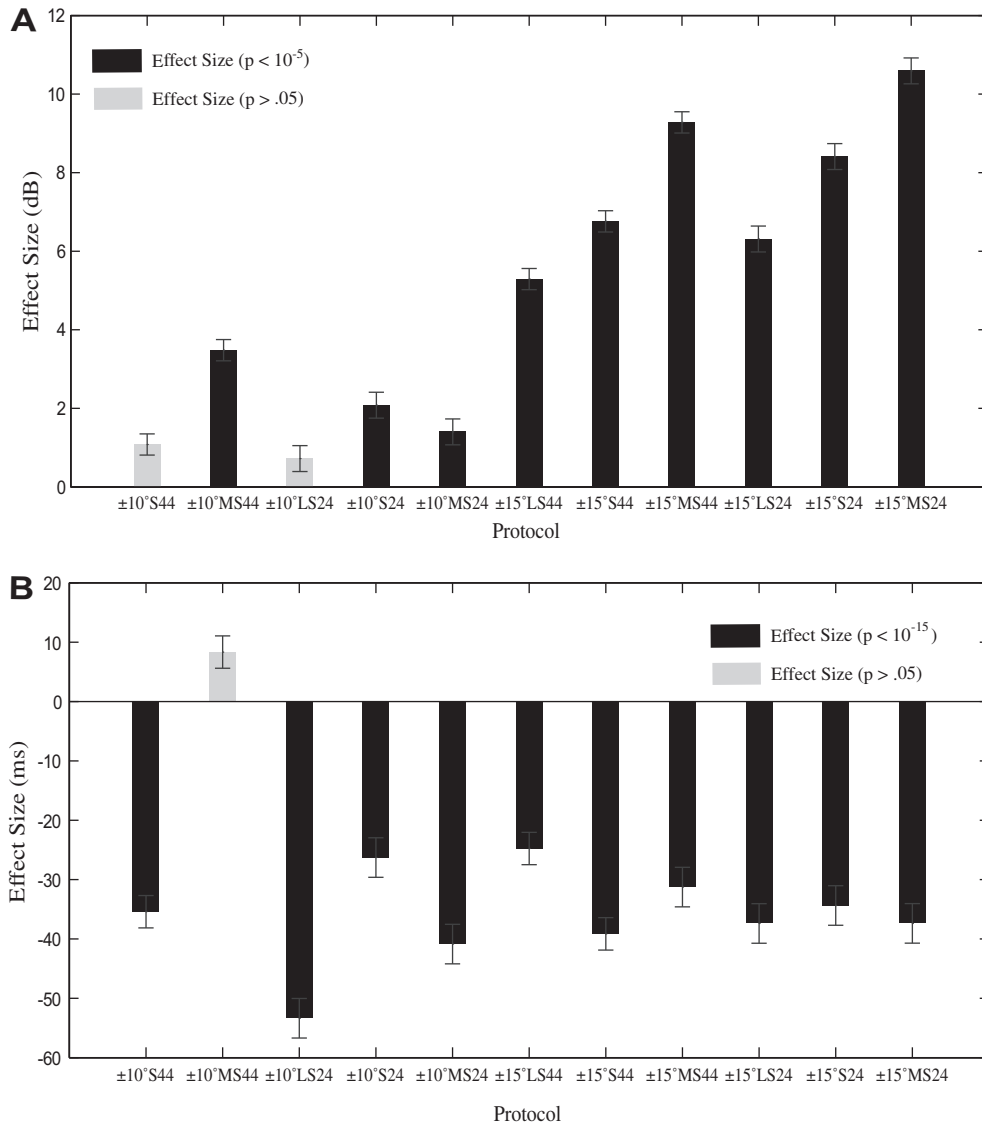

Fig. 4. Independent effect size across 11 separate stimulus conditions estimated by multivariate linear model for (A) pupil constriction amplitudes (dB) and (B) time to peak constriction (ms). Effect values represent deviations from the reference response protocol ± 10° visual field LS44.
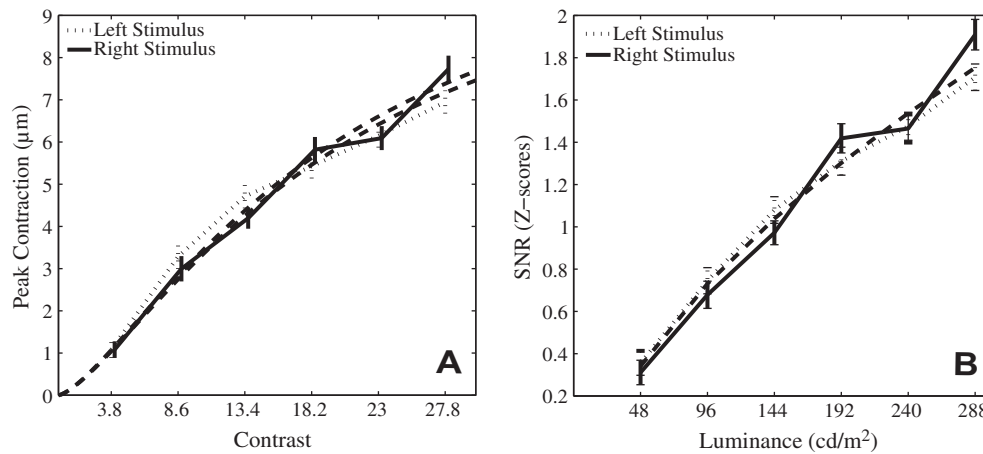
Fig. 5. (A) The stimulus response function characterizing median pupillary constriction amplitudes (median of right and left pupil contraction for each stimulus protocol) over a range of luminance contrast was fit to the data using the Naka–Rushton equation. (B) The effect of luminance intensity on median SNRs. Amplitude of pupil responses and SNRs both identify saturation at higher luminances.

response saturation to be a feature of all visual field regions when stimuli at high luminances were presented (Maddess et al., 2010). We also examined time to peak contraction as a function of luminance and found that mean latency grows shorter with increasing luminance for normal subjects from 524.1 ± 6.4 ms for stimulus luminance 48 cd/m^2 to 478.9 ± 5.2 ms for luminance 288 cd/m^2.

Analyses of the mean effects for each region for each of the six stimulus luminance intensities were undertaken by fitting the linear model to regional amplitudes (Fig. 6). The largest mean effects were found in the outer ring corresponding to regions outside the central 10° of visual field, and this was a general feature across all protocols (Fig. 6). With higher luminance levels, the mean regional peak response independent of other effects, increased and exhibited saturation at the upper end of the range.

4. Discussion

In this study, we examined the change in the response function of the pupillary light reflex according to field location, sampling density, temporal stimulus factors and luminance saturation. Overall slower stimuli subtending ±15° of the central visual field seemed to give responses that gave reasonable SNRs (i.e. median z-scores > 2), suggesting that such stimuli would be useful for quantifying visual field changes corresponding to the central retina. In addition to measurements of visual field sensitivity as represented by response amplitude the multifocal stimulation technique enabled us to quantify direct and consensual responses at each perimetric location and provide response delay, as well as standard errors for each amplitude and delay at every location. The multifocal methods helped achieve the reasonable SNRs because with concurrent presentation of the stimuli the measured responses were effectively the average of up to 240 pulses per region collected within a 4 min test period (eight segments of 30 s recordings). The median amplitude of contraction was variable between protocols with the 15°MS24 stimulus eliciting responses over 11 times larger than the 10 °LS44 stimulus.

Melanopsin-containing, intrinsically photosensitive retinal ganglion cells (ipRGCs) have recently been described as the predominant origin of all retinal input to the pupil response (Gamlin et al., 2007). In primates the pretectal olivary nucleus (PON) receives comparable input from ipRGCs and cortical structures (Gamlin et al., 2007). The PON is the main input into the Edinger–Westphal nucleus (EWN) (Gamlin, 2006) and subsequently to the ciliary ganglion which completes the parasympathetic reflex loop. The response characteristics of ipRGCs include both a transient yellow-on (M + L) /blue-off (-S) cone mediated response, and a separate sustained intrinsic melanopsin response with a peak sensitivity around 482 nm (Dacey et al., 2005). As it is now becoming clear that ipRGC are responsible for the transmittance of the pupillary signal from the retina (Guler et al., 2008), consideration must be given to their effect upon the pupil sensitivity profile. It is important to note that the stimulus parameters used in the present experiments are unlikely to activate the intrinsic component of ipRGC which operates with much slower dynamics than inputs through the photoreceptors. Finally, pupillary field defects may be influenced by pathological/aging damage to ipRGCs and much remains unknown about the resilience of ipRGCs to outer and inner retinal disease in humans, although one study from a rat model suggests that ipRGCs are less susceptible to injury from raised IOP than other ganglion cells (Li et al., 2006).

In agreement with previous studies (Tan et al., 2001; Wilhelm et al., 2000) the largest responses were found to be in the temporal field. These observations are concordant with retinal ganglion cell (RGC) topography of higher densities in temporal regions in the human retina (Curcio & Allen, 1990). This predominance for the temporal visual field has also been found in cat retinotectal pathways (Sterling, 1973). In primates evidence of nasal-temporal asymmetry has been noted in RGC density (Stone & Johnston, 1981) and dendritic field size (Silveira et al., 2004). This systematic bias favouring the nasal retina persists in primates to the cortical and subcortical projections (Williams, Azzopardi, & Cowey, 1995) and area V1 inputs (Tychsen & Burkhalter, 1997). Similar dichotomies have not been found to extend to the lateral geniculate nucleus (LGN) or cortical areas V1–V3 in humans identified by fMRI utilizing a 13° radius wedge stimulus (Sylvester, Josephs, Driver, & Rees, 2007). Thus, increased effect sizes of pupillary responses to temporal hemifield stimuli, as observed here, might be mediated by extra-geniculate pathways. A related study from this group found that the shape of stimulus response functions obtained to different colors of stimuli seem to depend only the stimulus luminance and not their color (Maddess et al., 2010).

Stimuli with low resolution layouts (e.g., 24 rather than 44 regions/field) may produce large median responses because on average they contain larger stimuli than the denser stimulus ensembles, and so on average recruit a greater population of receptors modulating the neural firing rate. Alternatively, the limited capacity of the pupil response resulted in a reduction of the overall response available to each region when stimulus ensembles with a larger number of regions were presented.
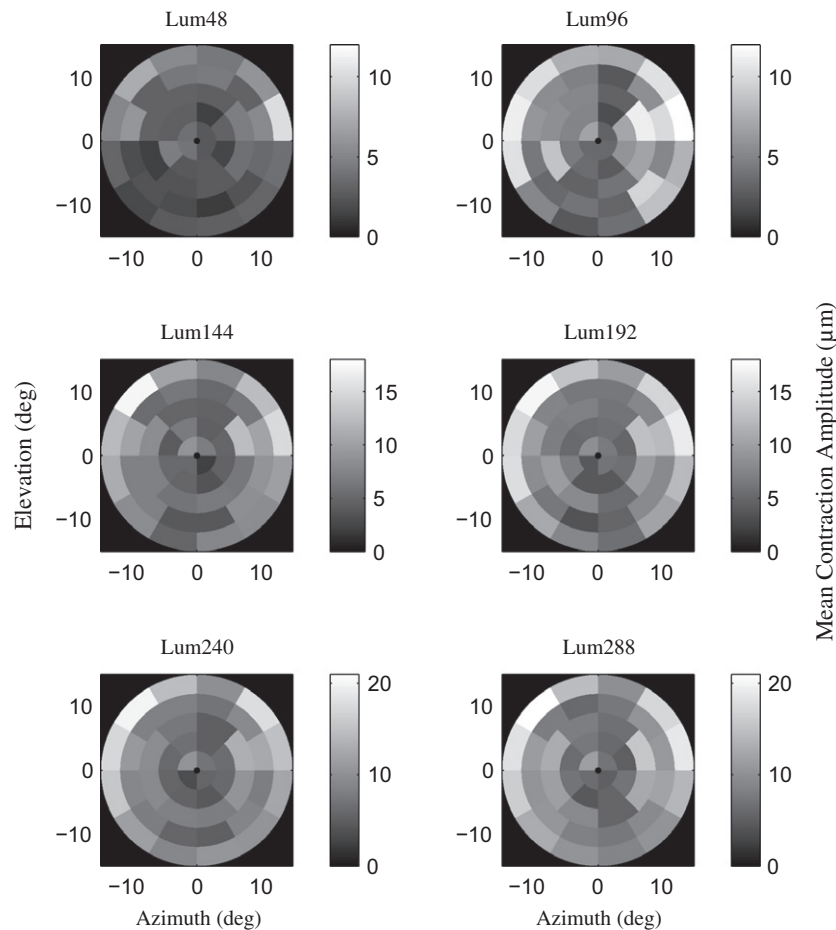
Fig. 6. Independent regional mean effects on response amplitudes calculated from linear models for six luminance intensities for stimulus ensembles subtending ±15° visual field. Responses from the right eye have been flipped and combined with left eye responses such that all data is presented as if they were from left eyes, therefore the temporal visual field is on the left. The background has been set to zero response. The titles of each panel refer to the stimulus luminance in cd/m².

The present study pointed to an increase in response size and reduced latency as a function of the sparseness of the stimulus presentation rate (Fig. 3). The ±15°MS24 stimulus elicited the largest responses and shortening the presentation interval tended to decrease the response size. Moreover, the non-overlapping low resolution layout of this stimulus consistently produced larger SNRs at each equivalent presentation rate. It was also found that extending the stimulus ensemble to ±15° eccentricity tended to achieve greater consistency of contraction amplitudes (Fig. 4A) providing good SNRs. It is conceivable that extending the stimulus field size further may increase amplitudes and SNRs from current levels. It is also possible that reducing the interval of presentation may expose variations in the pupillary waveform that would better correlate with pathological dysfunction.

Our purpose in limiting the field size to ±15° eccentricity was twofold. The first was to determine the optimal stimulus parameters for objective multifocal pupillographic assessment of macular pathology. Second was our desire to maintain a test paradigm that was clinically proficient, which limited our testing duration. Hence, determining the optimal sparseness without increasing test duration required a balance between response size and SNR.

The distinction between stimulus parameters that produce a large SNR versus large diagnostic power must also be considered. Low resolution stimuli, as illustrated in Fig. 1B, that produce larger pupil contractions may not offer as much detail regarding the anatomical borders of pathology relative to that attainable using a high resolution layout (Fig. 1A). This impairment is due to the limited capacity of the pupil to respond to stimuli. Regional signals

converge into a single signal from each pupil which is highly correlated between eyes. The effect is that highly responsive regions suppress others so it is conceivable that the variability in response from dysfunctional RGC within certain regions may not significantly impact the mean response. Consequently, diffuse loss of RGC may be indistinguishable from a small severe scotoma. The alternative is to use the 24 region stimulus strategy as a screening method and the 44 region stimulus ensemble for determining the extent and severity of scotomas. There may be arguments for the use of short and long wavelength light to differentiate the source of retinal dysfunction using the pupillary responses. Our use of a yellow stimulus was to minimize the effects of preretinal optical factors as the predominance of perimetry patients are affected by such factors (Weale, 1988).

Saturation of pupil sensitivity (Hong et al., 2001) has been reported by others, but we extend these observations to a multifocal stimulus array. Fig. 6 illustrates that response saturation is a general feature across all regions. The result implies that using high luminance stimuli may impair the ability to detect damage. The stimulus response curve becomes non-linear at the brighter intensities (Fig. 5A and B) flattening the contraction amplitude and SNR response profile. Thus, saturating luminances must be avoided; however, varying the level of luminance across the pupillary field may serve to balance responses. Such an approach would deliver brighter stimuli to less sensitive regions of the field and recent work in our lab has demonstrated an increase in median SNR and sensitivity and specificity for glaucoma (Kolic, Maddess, Essex, & James, 2009; Maddess, Kolic, Essex, & James, 2009b).

In conclusion, we have demonstrated the effect of temporal and spatial stimulus variants on the median multifocal pupillary light responses in an attempt to improve diagnostic accuracy. Median SNRs ranged from 1.67 to 2.47 with most sparse presentation rates. Pupil response saturation was evident with contraction amplitudes becoming less sensitive at the highest intensity. Sparse presentation intervals with low resolution non-overlapping ensembles produced the largest effect on response amplitudes and reduced time to peak contraction. Investigations measuring the diagnostic power of multifocal pupillography for age-related macular degeneration utilizing the optimal stimulus parameter derived from the present experiment are currently in progress.

Acknowledgment

References

Artes, P., Iwase, A., Ohno, Y., Kitazawa, Y., & Chauhan, B. (2002). Properties of perimetric threshold estimates from full threshold, SITA standard, and SITA fast strategies. *Investigative Ophthalmology and Visual Science, 43*, 2654–2659.

Bell, A., James, A. C., Kolic, M., Essex, R. W., & Maddess, T. (2010). Dichoptic multifocal pupillography reveals afferent visual field defects in early type 2 diabetes. *Investigative Ophthalmology and Visual Science, 51*(1), 602–608.

Bergamin, O., Zimmerman, M. B., & Kardon, R. H. (2003). Pupil light reflex in normal and diseased eyes: Diagnosis of visual dysfunction using waveform partitioning. *Ophthalmology, 110*(1), 106–114.

Bjerre, A., Grigg, J. R., Parry, N. R., & Henson, D. B. (2004). Test-retest variability of multifocal visual evoked potential and SITA standard perimetry in glaucoma. *Investigative Ophthalmology and Visual Science, 45*(11), 4035–4040.

Budenz, D. L., Rhee, P., Feuer, W. J., McSoley, J., Johnson, C. A., & Anderson, D. R. (2002). Sensitivity and specificity of the Swedish interactive threshold algorithm for glaucomatous visual field defects. *Ophthalmology, 109*(6), 1052–1058.

Chauhan, B. C., & Johnson, C. A. (1999). Test-retest variability of frequency-doubling perimetry and conventional perimetry in glaucoma patients and normal subjects. *Investigative Ophthalmology and Visual Science, 40*(3), 648–656.

Chen, P. P., & Budenz, D. L. (1998). The effects of cataract extraction on the visual field of eyes with chronic open-angle glaucoma. *American Journal of Ophthalmology, 125*(3), 325–333.

Cox, T. A., & Drewes, C. P. (1984). Contraction anisocoria resulting from half-field illumination. *American Journal of Ophthalmology, 97*(5), 577–582.

Curcio, C. A., & Allen, K. A. (1990). Topography of ganglion cells in human retina. *Journal of Comparative Neurology, 300*(1), 5–25.

Dacey, D. M., Liao, H. W., Peterson, B. B., Robinson, F. R., Smith, V. C., Pokorny, J., et al. (2005). Melanopsin-expressing ganglion cells in primate retina signal color and irradiance and project to the LGN. *Nature, 433*(7027), 749–754.

Gamlin, P. D. (2006). The pretectum: Connections and oculomotor-related roles. *Progress in Brain Research, 151*, 379–405.

Gamlin, P. D., McDougal, D. H., Pokorny, J., Smith, V. C., Yau, K. W., & Dacey, D. M. (2007). Human and macaque pupil responses driven by melanopsin-containing retinal ganglion cells. *Vision Research, 47*(7), 946–954.

Goldberg, I., Graham, S. L., & Klistorner, A. I. (2002). Multifocal objective perimetry in the detection of glaucomatous field loss. *American Journal of Ophthalmology, 133*(1), 29–39.

Guler, A. D., Ecker, J. L., Lall, G. S., Haq, S., Altimus, C. M., Liao, H. W., et al. (2008). Melanopsin cells are the principal conduits for rod-cone input to non-image-forming vision. *Nature, 453*(7191), 102–105.

Heijl, A., Lindgren, A., & Lindgren, G. (1989). Test-retest variability in glaucomatous visual fields. *American Journal of Ophthalmology, 108*(2), 130–135.

Henson, D. B., Evans, J., Chauhan, B. C., & Lane, C. (1996). Influence of fixation accuracy on threshold variability in patients with open angle glaucoma. *Investigative Ophthalmology and Visual Science, 37*(2), 444–450.

Hong, S., Narkiewicz, J., & Kardon, R. H. (2001). Comparison of pupil perimetry and visual perimetry in normal eyes: Decibel sensitivity and variability. *Investigative Ophthalmology and Visual Science, 42*(5), 957–965.

Hood, D. C., Greenstein, V. C., Holopigian, K., Bauer, R., Firoz, B., Liebmann, J. M., et al. (2000). An attempt to detect glaucomatous damage to the inner retina with the multifocal ERG. *Investigative Ophthalmology and Visual Science, 41*(6), 1570–1579.

Hood, D. C., & Zhang, X. (2000). Multifocal ERG and VEP responses and visual fields: Comparing disease-related changes. *Documenta Ophthalmologica, 100*(2–3), 115–137.

Hood, D. C., Zhang, X., Greenstein, V. C., Kangovi, S., Odel, J. G., Liebmann, J. M., et al. (2000). An interocular comparison of the multifocal VEP: A possible technique for detecting local damage to the optic nerve. *Investigative Ophthalmology and Visual Science, 41*(6), 1580–1587.

James, A. C., Maddess, T., Goh, X., & Winkles, N. (2005a). Spatially sparse pattern-pulse stimulation enhances multifocal visual evoked potential analysis. *ARVO – IOVS, 46* (pp. E-Abstract 3602). Ft. Lauderdale.

James, A. C., Ruseckaite, R., & Maddess, T. (2005b). Effect of temporal sparseness and dichoptic presentation on multifocal visual evoked potentials. *Visual Neuroscience, 22*(1), 45–54.

Joson, P. J., Kamantigue, M. E., & Chen, P. P. (2002). Learning effects among perimetric novices in frequency doubling technology perimetry. *Ophthalmology, 109*(4), 757–760.

Kardon, R. H., Kirkali, P. A., & Thompson, H. S. (1991). Automated pupil perimetry. Pupil field mapping in patients and normal subjects. *Ophthalmology, 98*(4), 485–495 (discussion 495–486).

Kim, Y. Y., Kim, J. S., Shin, D. H., Kim, C., & Jung, H. R. (2001). Effect of cataract extraction on blue-on-yellow visual field. *American Journal of Ophthalmology, 132*(2), 217–220.

Klistorner, A., & Graham, S. L. (2000). Objective perimetry in glaucoma. *Ophthalmology, 107*(12), 2283–2299.

Kolic, M., Maddess, T., Essex, R. W., & James, A. C. (2009). Attempting balanced multifocal pupillographic perimetry. *ARVO – IOVS, 50* (pp. E-Abstract 5280). Ft. Lauderdale.

Lai, T. Y., Chan, W. M., Lai, R. Y., Ngai, J. W., Li, H., & Lam, D. S. (2007). The clinical applications of multifocal electroretinography: A systematic review. *Survey of Ophthalmology, 52*(1), 61–96.

Li, R. S., Chen, B. Y., Tay, D. K., Chan, H. H., Pu, M. L., & So, K. F. (2006). Melanopsin-expressing retinal ganglion cells are more injury-resistant in a chronic ocular hypertension model. *Investigative Ophthalmology and Visual Science, 47*(7), 2951–2958.

Maddess, T., Bedford, S. M., Goh, X. L., & James, A. C. (2009a). Multifocal pupillographic visual field testing in glaucoma. *Clinical and Experimental Ophthalmology, 37*(7), 678–686.

Maddess, T. L., Kolic, M., Essex, R. W., & James, A. C. (2009b). Balanced luminance multifocal pupillographic perimetry. *ARVO – IOVS, 50* (pp. E-Abstract 5281). Ft. Lauderdale.

Maddess, T., Ho, Y. -L., Wong, S. S. Y., Kolic, M., Goh, X. -L., Carle, C. F., & James, A. C. (2010). Multifocal pupillographic perimetry with white and colored stimuli. *Journal of Glaucoma*, doi:10.1097/IJG.1090b1013e3181efb1097 (Epub ahead of print).

Maddess, T., James, A. C., & Bowman, E. A. (2005). Contrast response of temporally sparse dichoptic multifocal visual evoked potentials. *Visual Neuroscience, 22*(2), 153–162.

Silveira, L. C., Saito, C. A., Lee, B. B., Kremers, J., da Silva Filho, M., Kilavik, B. E., et al. (2004). Morphology and physiology of primate M- and P-cells. *Progress in Brain Research, 144*, 21–46.

Smith, S. A., & Smith, S. E. (1980). Contraction anisocoria: Nasal versus temporal illumination. *British Journal of Ophthalmology, 64*(12), 933–934.

Sterling, P. (1973). Quantitative mapping with the electron microscope: Retinal terminals in the superior colliculus. *Brain Research, 54*, 347–354.

Stone, J., & Johnston, E. (1981). The topography of primate retina: A study of the human, bushbaby, and new- and old-world monkeys. *Journal of Comparative Neurology, 196*(2), 205–223.

Sutter, E. E., & Tran, D. (1992). The field topography of ERG components in man—I. The photopic luminance response. *Vision Research, 32*(3), 433–446.

Sylvester, R., Josephs, O., Driver, J., & Rees, G. (2007). Visual FMRI responses in human superior colliculus show a temporal-nasal asymmetry that is absent in lateral geniculate and visual cortex. *Journal of Neurophysiology, 97*(2), 1495–1502.

Tan, L., Kondo, M., Sato, M., Kondo, N., & Miyake, Y. (2001). Multifocal pupillary light response fields in normal subjects and patients with visual field defects. *Vision Research, 41*(8), 1073–1084.

Tychsen, L., & Burkhalter, A. (1997). Nasotemporal asymmetries in V1: Ocular dominance columns of infant, adult, and strabismic macaque monkeys. *Journal of Comparative Neurology, 388*(1), 32–46.

Weale, R. A. (1988). Age and the transmittance of the human crystalline lens. *Journal of Physiology, 395*, 577–587.

Wilhelm, H., Neitzel, J., Wilhelm, B., Beuel, S., Ludtke, H., Kretschmann, U., et al. (2000). Pupil perimetry using M-sequence stimulation technique. *Investigative Ophthalmology and Visual Science, 41*(5), 1229–1238.

Williams, C., Azzopardi, P., & Cowey, A. (1995). Nasal and temporal retinal ganglion cells projecting to the midbrain: Implications for "blindsight". *Neuroscience, 65*(2), 577–586.

Wong, A. M., & Sharpe, J. A. (2000). A comparison of tangent screen, goldmann, and humphrey perimetry in the detection and localization of occipital lesions. *Ophthalmology, 107*(3), 527–544.

Young, R. S., & Kennish, J. (1993). Transient and sustained components of the pupil response evoked by achromatic spatial patterns. *Vision Research, 33*(16), 2239–2252.